PHILOSOPHICAL TRANSACTIONS
OF THE ROYAL SOCIETY A
MATHEMATICAL, PHYSICAL AND ENGINEERING SCIENCES

Anatomy of a glacial meltwater discharge event in an Antarctic Cove

Journal:	*Philosophical Transactions A*
Manuscript ID	RSTA-2017-0163.R1
Article Type:	Research
Date Submitted by the Author:	n/a
Complete List of Authors:	Meredith, Michael; British Antarctic Survey, Falk, Ulrike; Universitat Bremen; Alfred-Wegener-Institut Helmholtz-Zentrum fur Polar- und Meeresforschung Bers, Valeria; Alfred-Wegener-Institut Helmholtz-Zentrum fur Polar- und Meeresforschung; Leibniz Zentrum für Marine Tropenforschung Mackensen, Andreas; Alfred-Wegener-Institut Helmholtz-Zentrum fur Polar- und Meeresforschung Schloss, Irene; Instituto Antártico Argentino; Centro Austral de Investigaciones Cientificas; Universidad Nacional de Tierra del Fuego Ruiz Barlett, Eduardo; Instituto Antártico Argentino Jerosch, Kerstin; Alfred-Wegener-Institut Helmholtz-Zentrum fur Polar- und Meeresforschung Silva Busso, Adrián; Universidad de Buenos Aires Abele, Doris; Alfred-Wegener-Institut Helmholtz-Zentrum fur Polar- und Meeresforschung
Issue Code (this should have already been entered but please contact the Editorial Office if it is not present):	WAP
Subject:	Geochemistry (78) < CHEMISTRY (1002), Atmospheric science < EARTH SCIENCES, Biogeochemistry < EARTH SCIENCES, Glaciology < EARTH SCIENCES, Oceanography < EARTH SCIENCES, Meteorology < EARTH SCIENCES
Keywords:	Glacial discharge, Antarctica, Geochemical tracers, Stable isotopes

Anatomy of a glacial meltwater discharge event in an Antarctic Cove

Michael P. Meredith[1*], Ulrike Falk[2,3], Anna Valeria Bers[3,4], Andreas Mackensen[3], Irene Schloss[5,6,7], Eduardo Ruiz Barlett[5], Kerstin Jerosch[3], Adrián Silva Busso[8], Doris Abele[3]

[1] British Antarctic Survey, High Cross, Madingley Road, Cambridge CB3 0ET, United Kingdom

[2] University of Bremen, Bremen, Germany

[3] Alfred Wegener Institute, Helmholtz Centre for Polar and Marine Research, Am alten Hafen 24 / Am Handelshafen 12, 27570 Bremerhaven, Germany

[4] Now at: Leibniz-Centre for Tropical Marine Research, Bremen, Germany

[5] Instituto Antártico Argentino, Buenos Aires, Argentina

[6] Centro Austral de Investigaciones Científicas (CADIC, CONICET), Ushuaia, Argentina

[7] Universidad Nacional de Tierra del Fuego, Ushuaia, Argentina

[8] University of Buenos Aires, Argentina

(*corresponding author: mmm@bas.ac.uk)

Keywords: glacial discharge, Antarctica, geochemical tracers, stable isotopes.

Summary (no more than 200 words)

Glacial meltwater discharge from Antarctica is a key influence on the marine environment, impacting ocean circulation, sea level, and productivity of the pelagic and benthic ecosystems. The responses elicited depend strongly on the characteristics of the meltwater releases, including timing, spatial structure and geochemical composition. Here we use isotopic tracers to reveal the time-varying pattern of meltwater during a discharge event from the Fourcade Glacier into Potter Cove, northern Antarctic Peninsula. The discharge is strongly dependent on local air temperature, and accumulates into an extremely thin, buoyant layer at the surface. This layer showed evidence of elevated turbidity, and responded rapidly to changes in atmospherically-driven circulation to generate a strongly pulsed outflow from the cove to the broader ocean. These characteristics contrast with those further south along the Peninsula, where strong glacial frontal ablation is driven oceanographically by intrusions of warm deep waters from offshore. The Fourcade Glacier switched very recently to being land-terminating; if retreat rates elsewhere along the Peninsula remain high and glacier termini progress strongly landward, the structure and impact of the freshwater discharges are likely to increasingly resemble the patterns elucidated here.

1. Introduction

Since the middle of the last century, the West Antarctic Peninsula (WAP) has shown strong atmospheric warming, with marked variability and periods of cooling superposed (1). Rates of warming up to the late 1990s were amongst the strongest globally, and were associated with rapid retreats of sea ice, surface ocean warming, and a shortening of the sea ice season (2–4). Whilst rates of change have subsequently been markedly lower, the WAP remains an area of profound interest concerning climatic change and its impacts on the marine environment (5). Concurrent with the atmospheric and sea ice changes has been a retreat of the majority of marine-terminating glaciers along the WAP, and a recent acceleration in their retreat rates (6). This was initially presumed to be causally linked to the atmospheric warming and southward progression of isotherms, but it was recently shown that strongest retreats have occurred predominantly in the central/southern WAP region where intrusions of warm, deep water from offshore can penetrate across the shelf and undercut the marine termini of the glaciers (7). Further north on the WAP shelf, where deep waters are significantly cooler, there is not the same consistent pattern of retreat, nonetheless these glaciers remain of significant influence not least because of the physical and geochemical influence they exert on the ocean (8,9).

At the very northern tip of the WAP, the area of Bransfield Strait and the South Shetland Islands (Figure 1) is influenced atmospherically by the westerly winds that overlie the Southern Ocean, and which have been intensifying in recent decades as a consequence of more frequent positive phases of the summer Southern Annular Mode (SAM) (10). These winds drive warm and moist air toward and across the northern WAP, where they cause surface thinning and disintegration of the coastal ice shelves with resulting acceleration of the coastal marine and tidewater glaciers (11,12). Once the buttressing ice shelf has been removed, the speed of glacial mass loss becomes a function of surface and basal melting rates of the local ice sheet margins. Atmospheric warming and precipitation cause surface thinning and meltwater infiltrations into the icecap which add to basal meltwater formation and accelerate glacial ice flow (13). Glaciers on the smaller island ice caps, such as on King George Island/25 de Mayo (KGI; Figure 1), are currently retreating at unprecedented speed (14,15). The immediate consequences of glacier and ice sheet loss at the northern WAP are diverse, and include a modification of ocean stratification and circulation, and changes to oceanic light levels and primary productivity (16). Furthermore, the Peninsula glaciers north of 70 °S have the potential to raise sea level by 69 ± 5 mm (17).

The occurrence of extended meltwater plumes from northern WAP glaciers can transport large quantities of lithogenic particles derived from subglacial erosion and ice-free surface outwash into near coastal and shelf areas. This can represent an enhancement of micronutrient supply to the near-coastal and High Nutrient/Low Chlorophyll regions of the Southern Ocean (18), especially the bioavailable forms of iron (8). Increased appreciation of the importance of these phenomena has led to renewed interest in determining the key processes and impacts that occur in the coves and fjords that connect the northern WAP glaciers to the broader ocean, and which are currently insufficiently understood and often inadequately represented in models.

A long-term interdisciplinary research program at KGI has focused on the multiple drivers and interactive effects of the melting Fourcade Glacier that drains into its coastal fjord, Potter Cove, and from there transiting Maxwell Bay into Bransfield Strait (Figure 1). The Fourcade Glacier is currently retreating at around 40 ma^{-1}, becoming land-terminating in 2016. Potter Cove circulation is generally cyclonic, and is influenced by the circulation of the adjacent Maxwell Bay that reaches down to 500 m depth (19,20). Strong katabatic winds can mix the water column down to the seabed, which can resuspend the soft sediments present in the inner cove. Horizontal circulation is noted to be significantly wind-forced, with indications of upwelling of deep waters in the cove's inner part under northeasterly winds, whilst tides may be significant in modulating circulation during periods of comparatively weak wind forcing (< 4 ms^{-1}) (20).

Approximately 20,700 m^3 of glacier ice is discharged into Potter Cove per day during the melt season, with a broadly comparable amount of meltwater drainage (21). A turbid freshwater layer approximately 5 m thick forms at the surface of the cove during the melt season. This layer is generated by cascading glacial surface melt and subglacial meltwater entering the inner cove mainly in its northeastern section where the receding ice was, at the time of sampling, still directly bordering and adjacent to the water (marked white in Figure 1, with brown areas indicating ice-free coastal areas). Floating ice blocks and brash ice, melting within the plume or onshore, enhance the freshness of this surface layer. Mixed discharge of surface and subterraneal meltwater streams entering Potter Cove at its southern coastline (9). Part of the subterraneal discharge occurs at shallow depths and is a source of bioavailable aqueous Fe(oxyhydr)oxides or reactive ferrihydrite nanoparticles to the shallow mixed layer (22,23). Subglacial iron-bearing meltwaters and iron leaching from suboxic coastal and shelf sediments at the South Shetland Islands (SSI) is an important source for natural fertilization of the Scotia Sea through advective transport (24,25).

Locally, the turbid meltwaters tend to have an adverse effect on productivity by restricting light penetration into the seawater, thus constraining benthic and pelagic primary production in the water column. Potter Cove has thus traditionally been regarded as a low productivity ecosystem with short bloom events, sometimes lasting only a few days to weeks, with maximum Chl-a values around 4 mg m^{-3} (26). Strong bloom events are seen only after very cold winters (e.g. El Niño years) when late disintegration of coastal sea ice stabilizes surface stratification before the onset of glacial discharge flow (16). Only few macroalgal species colonising clear water areas in the outer cove are found on the newly ice-free hard substrates in glacial vicinity; these species need to be adapted to low light conditions to manage with only a short growth period in early spring (27). Species adapted to low light are also typical representatives of the pelagic microbial pro- and eukaryote communities (see (28) for review).

There is thus a strong need to understand better the physical drivers and ecological impacts of glacial discharge into coves and fjords at localities such as the northern WAP. Accordingly, we conducted a short, dedicated sampling programme to resolve the three-dimensional structure of the glacial meltwater plume in Potter Cove and the opening into Maxwell Bay with unprecedented spatial and temporal resolution. Serendipitously, this programme captured the initiation, evolution and fate of a pronounced meltwater discharge and outflow event, and hence offers unique insight into the drivers and controls on the glacially-derived freshwater.

2. Methods

2.1. Sample and water column data collection

Water samples for oxygen isotope analysis were collected at four depths (0, 5, 10 and 20 m) along transects across Potter Cove and Maxwell Bay, using 4.7 litre Niskin bottles. Concurrent water column profiling was conducted using a Sea-Bird SBE 19 Conductivity–Temperature–Depth (CTD) instrument, with an auxiliary sensor of turbidity ECO NTU. Salinity profiles were derived from the CTD data, and values extracted from the levels corresponding to the depths of the water sampling. Turbidity data were here averaged over the upper 3 m of the water column for analysis. Sampling events were conducted on each of 6, 11, 13 and 16 February 2013. The spatial pattern of sampling and data coverage is indicated by the distributions of salinity and isotopes shown in Figures 2 and 3.

2.2. Oxygen isotope measurement

From each Niskin event, samples of 100 ml water were drawn into glass vials, sealed with wax, and stored at 4 °C temperature prior to analysis. In the laboratory, 7 ml of water were equilibrated in 13 ml headspace with CO_2 gas using a Finnigan equilibration device. Oxygen isotope equilibrium in the CO_2–H_2O system was attained by shaking for 430 min at 20 °C. The equilibrated gas was purified and transferred to a Finnigan Delta-S gas mass spectrometer. Sample preparation and isotope measurements were calibrated against Vienna Standard Mean Ocean Water (VSMOW) and Standard Light Antarctic Precipitation (SLAP) standard waters. At least two replicates (including preparation and measurement) were run for each oxygen isotope determination. Results are reported in δ-notation ($\delta^{18}O$)

versus VSMOW with a mean precision better than ±0.03 ‰. Fuller details are provided in (29).

2.3. Identification and quantification of meteoric water

The benefit of $\delta^{18}O$, when measured in addition to salinity, is that it permits identification of meteoric-derived freshwater (i.e. that derived from glacial sources and/or precipitation) separately from sea ice melt. This is because both meteoric water injection to the ocean and sea ice production/melt have significant impacts on ocean salinity, whereas only the former has a significant impact on ocean $\delta^{18}O$. Fuller background on $\delta^{18}O$ as a freshwater tracer, and its application at the WAP, is available in (30).

For each $\delta^{18}O$ value, corresponding salinity was extracted from the CTD data and the pairs of data were used in a mass balance that presumes the composition of each sample to be a simple mixture of 3 components, namely sea ice melt (sim), meteoric water (met), and ocean water (ow):-

$$\begin{gathered} Fsim + Fmet + Fow = 1 \\ Ssim.Fsim + Smet.Fmet + Sow.Fow = S \\ \delta sim.Fsim + \ \delta met.Fmet + \ \delta ow.Fow = \ \delta \end{gathered} \qquad (1)$$

where Ssim, Smet, Sow are the endmember salinities of the source components; δsim, δmet, δow are the corresponding $\delta^{18}O$ values; and S, δ are the measured salinity and $\delta^{18}O$ of each sample. This system of equations is solved for Fsim, Fmet, Fow, which are the respective fractions of the 3 components in each sample collected.

Application of this method requires the endmember values of the unmixed source waters to be established. Here we use values of Sow = 34.40, δow = -0.2 ‰, following data presented in (31) for properties in Maxwell Bay. Smet is taken to be 0.0, and δmet is set to -11 ‰, following (32) and (33). This value varies from others used in isotopic studies further south along the WAP (30,34), consistent with the spatially-varying $\delta^{18}O$ structure of the Peninsula glaciers. We also use Ssim = 5, which is a reasonable approximate value for this region, and δsim is set as +1.6 ‰ to take into account fractionation processes upon sea ice formation. Typical uncertainties using this method are close to or less than ±1 % in the freshwater fractions quantified, and derive mainly from uncertainty in the meteoric water endmember choice (30).

2.4. Meteorological data

An Automatic Weather Station (AWS, Campbell Scientific, Logan USA) was installed at 62°14'09.8'' S, 58°36'48.7'' W (230 m above sea level) on the Fourcade Glacier, and operated from November 2010 until March 2017 (35). The AWS was designed to estimate all components of the surface energy balance equation and equipped with wind anemometers and vanes (Alpine Wind Monitor) at two heights, air temperature and relative humidity sensors (HMP155A), and five depths of snow and ice temperature measurements (107 Thermistor Probes) to derive sensible, latent and ground (ice) heat fluxes. The AWS included a four-component radiation sensor for up- and downwelling longwave and shortwave radiation fluxes (NR01), in addition to a SR50A Sonic Ranging Sensor installed at an initial height of 2 m to measure surface elevation changes. Levelling and adjustment of sensors were carried out at the start and end of each summer field campaign. In particular, the whole station needed to be lowered about 2 to 3 m at the end of the ablation season each year. Measurement rate was set to every 5 seconds with an averaging interval of 10 minutes.

2.5. Glacial discharge modelling

The meteorological data were aggregated to hourly values and gap-filled in order to force a glaciological melt model developed by (36) and adapted for the South Shetland Islands by (15) to assess glacial discharge from Fourcade Glacier into Potter Cove. The glacier melt model calculates the energy available for melt as the residual of the surface energy balance equation:

$$Q_M = G(1-\alpha) + L_N + Q_H + Q_L + Q_G + Q_R \tag{2}$$

where L_N is the longwave net balance, G the global radiation. The term $(1-\alpha)$ signifies the solar incidental radiation minus the part (α = albedo) reflected at the glacier surface. Q_H and Q_L are sensible and latent heat, respectively, and Q_G is the ground heat flux. Q_R is the sensible heat supplied by rain during phase transition from liquid to solid.

The energy balance equation is solved for each time step and each point on a spatial grid of 10 m by 10 m, taking into account the differing exposure of the glacier surface, zonal distinction of ablation and accumulation patterns (21) and surface properties and lapse rates of air temperature, precipitation and wind speed. The albedo α is defined by the surface' ablation and accumulation pattern and is configured to reflect the alteration of the

234 snow pack with time. The sum of computed melt and rain water is integrated over the
235 glacier catchment area, and defines the glacial discharge. Output of the model is glacier
236 discharge calculated on an hourly basis. Although calibration and validation processing show
237 a good agreement between model and observations, the processes of turbulence-driven
238 snow deposition, refreezing and wind drift are not taken into account by the model. The
239 model thus overestimates glacial discharge, predominantly at the end of the melt season,
240 i.e. March to May. Turbulence-driven snow deposition prevails in the vicinity of obstacles,
241 e.g. moraines and steep topography, and is confined locally. This process is not incorporated
242 in the model physics. It adds to the uncertainties in model output. During the here
243 considered time period, uncertainty in simulated glacial discharge can be assumed to be less
244 than 10%.
245
246 **3. Results**
247 **3.1 Isotopic structure of Potter Cove and Maxwell Bay waters**
248
249 The most spatially expansive sampling for oxygen isotopes and oceanographic parameters
250 was conducted on February 16th 2013, when a section was completed along the length of
251 Potter Cove and extending across Maxwell Bay to reach close to Nelson Island (Figure 2).
252 The freshest waters encountered were at the surface near the head of Potter Cove (salinity
253 around 33.0); waters were progressively more saline with depth and towards the centre and
254 western flank of Maxwell Bay, but with some slightly fresher waters (salinity around 33.9) at
255 surface close to Nelson Island (Figure 2a). This general pattern is mimicked by that of $\delta^{18}O$,
256 which had values around -0.5 to -0.6 ‰ at the surface near the head of Potter Cove, with
257 higher values (-0.3 to 0.4 ‰) at greater depths and extending toward the centre of Maxwell

Bay (Figure 2b). Adjacent to Nelson Island there is some evidence of isotopically lighter waters at the surface (-0.45 to -0.6 ‰).

Applying Equation 1 to these data reveals the spatial fields of sea ice melt and meteoric water (Figure 2c and 2d respectively); this demonstrates that meteoric water is strongly responsible for the low salinities observed at the surface of Potter Cove, with 3-5 % of the waters sampled being of meteoric origin at this time. Sea ice melt values are generally lower and more scattered, with slight negative values denoting small net sea ice production from the waters sampled relative to the endmembers chosen (Figure 2c).

These freshwater contributions are also evident when the data are viewed in salinity-$\delta^{18}O$ space (Figure 3d), which shows a cluster of points from the subsurface layers (red, green and blue dots) near S=34, $\delta^{18}O$=-0.35 ‰, but with the surface layer (black dots) showing an extension along the meteoric water mixing line, and with some points offset from this line slightly toward higher salinity. (The arrows in Figure 3c indicate the impact that freshwater inputs will have on the locus of data points, with sea ice melt (freeze) moving the locus horizontally to the left (right), whilst meteoric water injection would move the locus diagonally downward to the left.)

Also shown in Figure 3d are data points from a research cruise that was conducted in 2010 (ANDREX; 37), during which $\delta^{18}O$ was measured across Bransfield Strait and the northern Antarctic Peninsula shelf. The deeper ANDREX data (red asterisks; depths greater than 150m) show data that are more saline and isotopically heavier than were measured in the shallower layers across Maxwell Bay, however the shallower ANDREX data (blue asterisks;

depths less than 100m) lie on the same cluster near S=34, $\delta^{18}O$=-0.35 ‰. This indicates that the processes which mediate the general exchange of waters between Maxwell Bay and the adjacent shelf do not result in major water mass modification, and that water discharged from peripheral coves into Maxwell Bay can penetrate outwards to the broader shelf relatively uninhibited.

3.2 Changes in the composition of Potter Cove waters

Figure 3(a-d) shows the full sequence of data collected within Potter Cove during each of February 6, 11, 13 and 16 respectively. The general pattern of subsurface waters is consistent across each day of sampling, clustering on a comparatively saline, isotopically heavy point. In contrast, whilst data in the surface layers all extend toward fresher, isotopically lighter waters, the extent to which they do this varies dramatically. In particular, February 11th shows remarkably fresh, isotopically light surface properties (S < 28.0; $\delta^{18}O$ < -2.5 ‰) compared with preceding or subsequent days. Full-resolution CTD profile data (not shown) reveal this to be an extremely thin (<1 m) layer.

The spatial freshwater structure is evident in Figure 4, the most striking feature of which is the very low salinity layer that occupied the surface of most of Potter Cove on February 11th (Figure 4b). Whilst the previous sampling on February 6th (Figure 4a) was not as spatially extensive as that on February 11th, there was no evidence for this layer in the inner part of Potter Cove at that time. Just two days after its detection (February 13th; Figure 4c), the layer had disappeared, and there is evidence that salinities within the inner part of Potter Cove were elevated at depth relative to those observed prior to the layer's creation (c.f.

February 6th). More expansive sampling on February 16th (Figure 4d) revealed no evidence of the layer, and conditions were generally similar to those at the start of the data sequence (February 6th). The $\delta^{18}O$ data from the sequence of samplings (Figure 5) show patterns that strongly resemble the salinity data, consistent with the inferred dominance of meteoric water inputs in determining the freshwater structure of our data.

Using Equation 1, we quantify the meteoric water prevalence across Potter Cove as a function of time (Figure 6). This shows moderate values at the surface on February 6th (Figure 6a; maximum around 5 %), rising sharply to ~15-20 % on February 11th (Figure 6b) before dropping dramatically thereafter. Sea ice melt prevalences (not shown) are very much smaller throughout the full sequence of measurements, with values in the range -2 to +1 %; the oxygen isotopes thus confirm the negligible impact of sea ice in contributing to the freshwater event.

Turbidity also showed marked changes during our sequence of data (Figure 7). Initial values (February 6th; Figure 7a) were moderately low except at the very head of Potter Cove. When the strong freshwater layer occupied the surface of Potter Cove (February 11th), the turbidity values were generally higher (values around 10 NTU), with the exception of at the head of the cove (Figure 7b). Subsequent to the loss of the strong freshwater layer (February 13th and 16th; Figures 7c and 7d), the turbidity values in the cove declined, reaching a minimum on February 16th except in the immediate proximity of the glacier head where subglacial melt leaks into the cove.

3.3 Meteorological and glaciological forcings

Figure 8 shows the key meteorological data from the period under study, and the modelled meltwater discharge from the different components of the Potter Cove glacial system. Prior to our initial isotope sampling on February 6th, there had been a general rise in air temperature of 1-2 °C since the start of January 2013, though with significant variability superposed. Associated with this, there had been a general increase in meltwater discharge, with discharge from the snow area dominating.

The changes in air temperature were strongly coupled with variability in wind direction. In general, winds from the west are associated with advection of warm and moist air masses from mid latitudes, whereas winds from the east are associated with katabatic wind systems and the influence of the Antarctic high pressure cell. Between February 6th and 11th, winds were consistently from the west, air temperature remained above the freezing point, and the rate of total glacial discharge remained significant. Between February 11th and 13th, winds were predominantly from the east, the air temperature dropped significantly, and there was an associated marked decline in glacial discharge. After February 13th, the wind switched direction again, and became more variable.

The discharge calculated for the different source areas reveals the processes responsible for driving the discharge (Figure 8). The firn area is in the glacier's accumulation zone, with air temperatures that are mostly below zero, whilst the snow area encompasses all surface areas with snow from the preceding winter. The main driver is the air temperature, and, to a lesser degree, the radiation flux densities due to high albedos of fresh snow and firn (approximately 0.75-0.9). The discharge in the ice area is driven to a large extent by radiation fluxes due to its significantly lower albedo (as low as <0.1), whereas the rock area shows the response to precipitation events.

4. Discussion and Conclusions

Glacial discharge is known to exert a strong influence on marine physical, biogeochemical and ecological systems. A key factor that determines the nature of impact that glacial discharge will have is the depth at which it enters the ocean. Meltwater injected at depth may rise as a buoyant plume, but if it entrains oceanic water as it ascends it may reach a level of neutral buoyancy before it reaches the surface; at this point, the (bio)geochemical tracers contained therein may be restricted to lie below the euphotic zone. Conversely, meltwater discharged to the upper layers will likely reinforce stability and strengthen stratification, and tracers and particles contained therein could be retained in the near-surface layers more effectively, however strong mixing and lateral advection/dispersion will affect the fate and downstream impact of these meltwaters.

We have seen a marked example of the latter case, where a layer of glacially-derived meltwater flooded the surface of a northern Antarctic Peninsula cove, creating an extremely thin, buoyant, freshwater layer. Serendipitously, our sampling enabled the determination of the spatial structure of this layer across the cove and beyond, and, combined with the local meteorology and glaciology data, it also allowed the genesis, evolution and demise of the layer within the cove to be characterised.

Of significant note is the strongly episodic nature of the freshwater layer. This was caused by complex interactions of meteorological forcings. The discharge to the ocean is strongly dependent on atmospheric temperature, which fluctuates on characteristic weather timescales, as well as seasonal and longer periods. The build-up of the freshwater layer within the cove was initially promoted by retentive winds, but reversal of the wind direction then flushed the layer rapidly out of the cove into Maxwell Bay, and ultimately beyond.

Using conservative freshwater tracers allows us to quantify some key aspects of the glacial discharge. We find that average meteoric water percentages at the surface were of order 20 % during the sampling when the freshwater layer was present, so (very approximately) the pure meltwater released had mixed fivefold in the period over which it was released. This has implications for the concentration of other tracers within that layer, such as micronutrients, which would also have been subject to the same level of mixing.

During the 5 days between isotope samplings over which the freshwater layer built up (February 6 to 11), the average discharge into Potter Cove was around 2.5 $m^3 s^{-1}$. In the absence of any wind-forced export or mixing, this discharge over such an interval would create a layer ~15 cm thick at the ocean surface. This layer would be fivefold thicker if the water therein were mixed to 20 % of its initial pure freshwater state, as suggested by the isotopic mass balance calculation, or ~75 cm thick. It should be noted that discharge was non-zero for a couple of days prior to our initial isotope sampling on February 6th (Figure 8), and the values derived here are acknowledged to be very coarse. Despite this, overall the quantitative nature of the freshwater layer (including its thickness) is seen to be consistent with quantifications of the freshwater injected to the ocean.

The horizontal circulation changes alluded to above are only one aspect of the time-varying Potter Cove system. In addition, there is evidence that the vertical (overturning) circulation also responded to the changes in forcing identified herein. In particular, Figure 5 shows that concurrent with the export of isotopically light water from the surface of the cove during February 11 to 13th, there was an increase in $\delta^{18}O$ values in the subsurface layers. This water is also more saline, and must have been drawn into the cove from further offshore toward Maxwell Bay, since there was no deep water with comparable properties resident in Potter Cove up to that time. Following the end of the export event (February 16th; Figure 5d), there was an apparent relaxation back toward initial conditions at all depths, presumably due to slumping of internal ocean layers as the export-favourable surface wind stress reduced.

The loss of the surface fresh, isotopically light layer between February 11 and 13 is ascribed here to horizontal export, with minimal impact from vertical mixing. This is excluded on the grounds that the winds were actually no stronger during the period that the freshwater was exported than they were before that period (only the direction had changed), and the creation of the layer had not been impeded. Further, if the freshwater were being redistributed in the vertical as opposed to the horizontal, there would be no significant change in freshwater column inventories derived from the salinity profiles, which is not the case.

The depth over which the isotopic changes with opposing signs occurs is important: the outward export of fresh, isotopically light water is evidenced in the surface samples, but all samples below (5 m and deeper) show evidence of import of more saline, isotopically heavier waters to the cove. This identifies that whilst changing wind forcing has a significant impact on the speed and direction of the surface layer circulation in the cove, it also influences the deeper circulation in an opposing sense, with the "hinge point" for the accelerated overturning sitting above or close to 5 m depth.

It is possible to estimate the acceleration of the overturning circulation in the cove during the period of export-favourable winds, albeit very approximately. The volume of the inner cove is around 140×10^6 m^3; if this whole part of the cove were replenished over a 2 day period (February 11 to 13), this would require an overturning rate of 1600 $m^3 s^{-1}$ (or 1.6 mSv). It should be noted that this back-of-the-envelope calculation only represents the *minimum* overturning necessary to replenish the waters of the inner cove; the actual rate that occurred could have been significantly higher. Further, if one assumes a sill depth separating the inner cove of around 20 m, with a 2 km cove width at this point, one has an effective "flux gate" of 40,000 m^2 through which the exchanged waters must pass. Using this, a figure for mean speed of throughflow of around 4 cm/s can be derived which would be needed to support the overturning rate derived above. This can be compared with the efflux speed inferred for the period between February 11 and 13, during which the whole inner cove was cleared of isotopically light water. If the export distance were approximately 3 km, a minimum mean export speed of around 2 cm/s would be needed to flush the freshwater from the cove. Whilst both these calculations are necessarily very coarse, the approximate agreement lends credence to these results being credible ballpark figures for overturning and export rates.

Previous studies have used oxygen isotope tracers to elucidate the freshwater system, including at King George Island (e.g. 31); often such studies use single sampling events to characterise an area. Further south on the WAP, a long-term programme involves quasi-weekly sampling for oxygen isotopes, but normally only at a single site, and (until recently) with the bulk of the sampling conducted in the subsurface layer (15m; 30). The strong episodic nature of the freshwater system noted in our more extensive sampling highlights that such sampling protocols may miss key elements of the spatially- and temporally-varying system if applied without knowledge of the scales required to be resolved. This is important if dynamical drivers and their responses are to be correctly identified, and if their representation in models is to be determined as robust.

We have observed that the freshwater layer that capped Potter Cove on February 11th had generally elevated levels of turbidity, albeit with values not as extreme as individual points found close to the glacier on February 6th or 16th. It is presumed that this indicates some level of suspended particulate material being injected to the cove, though the levels observed suggest that the concentrations in the freshwater released may not have been very high. The fate of these particles when the freshwater layer is exported from the cove is not well determined, but will be some combination of lateral export and sinking to the seabed. Previous investigations using sediment traps in this locality found that between 15 and 50 % of suspended particulate material was exported horizontally (9). In both cases of high and low sediment export rates, however, there are significant potential consequences, especially if this general pattern of export is recurrent over multiple fjordic systems around the fringes of Antarctica. Strong injection of sediment to the ocean associated with glacial discharge has been associated with negative consequences for zooplankton, including mass mortality events for Antarctic krill (*Euphausia superba*); this was deduced using data collected within Potter Cove (38), where krill propulations have been notably absent in recent years. Further, the benthic ecosystem has also been demonstrated to be strongly impacted by sediment accumulation (39,40). The episodic discharge and flushing we have witnessed represents a layer of complexity in the delivery and export of this sediment, affecting the timescale of its retention within the cove, and its ultimate fate.

A key feature of our findings is the strong meteorological control of glacial meltwater discharge and efflux to the general shelf, as opposed to stronger oceanographic control further south. In particular, the delivery of the meltwater to the ocean appears heavily dependent on atmospheric temperature, and its fate in the ocean depends markedly on the directionality of the winds. Atmospheric warming on the WAP has recently undergone a period of hiatus associated with natural variability, but if the strong warming witnessed during the second part of the twentieth century resumes, one could potentially expect further accelerations of freshwater injection from systems comparable to Potter Cove. If the majority of the glaciers further south along the WAP continue to retreat landward, it is likely that such systems will progressively resemble more closely the one observed here.

The directionality of the winds has been identified as a key control in the fate of the freshwater. Whilst this is clearly dependent on the orientation of the cove studied, it is very possible that other coves will have similar dependencies, albeit potentially to different components of the vector winds. Like atmospheric temperature, winds at the Peninsula are known to be sensitive to large-scale modes of climatic variability, including the El Niño - Southern Oscillation phenomenon and the SAM (41). Each of these has long-period variability, including a decadal trend in the SAM that is known to be at least partly driven by greenhouse gas emissions and (in particular) ozone depletion. This raises the likelihood of long-period (decadal) changes in both the discharge and fate of freshwater released into Antarctic coves including an element driven by anthropogenic forcings.

Data Accessibility

Bathymetry data are available at https://doi.pangaea.de/10.1594/PANGAEA.853593.

Oceanographic (CTD) data are available at https://doi.org/10.1594/PANGAEA.869413.

Isotope data are available at https://doi.pangaea.de/10.1594/PANGAEA.884851.

Glaciological datasets are available at https://doi.org/10.1594/PANGAEA.874599.

Meteorological datasests are available at http://dx.doi.org/10.1594/PANGAEA.848704.

Competing Interests

The authors declare no financial or non-financial competing interests.

Authors' Contributions

Michael Meredith led the data analysis/interpretation and the writing of the paper; Andreas Mackensen conducted the oxygen isotope measurements; Ulrike Falk processed the meteorological data and conducted the glacial discharge simulations; Eduardo Ruiz Barlett and Anna Valeria Bers designed and implemented the sampling programme and initial sample/data handling. All authors contributed to the interpretation and discussion of the results, and approved the final version of the paper.

Acknowledgements

Oscar González and Marta Sierra are thanked for supporting the sampling programme and initial data processing. Lisa Schönborn and Günter Meyer are thanked for operation and maintenance of the mass spectrometer used for stable isotope determinations. Laura Gerrish is thanked for assistance with figure preparation.

Funding Statement

This study received support from the European Commission under the 7th Framework Programme through the Action – IMCONet (FP7 IRSES, action no. 318718). The participation of Michael Meredith in this research was funded by the Natural Environment Research Council via awards NE/N018095/1 and NE/P003060/1. Kerstin Jerosch acknowledges funding from AWI, DFG SSP 1158 Grant JE 680/1-1; Marie Curie Action FP 7 IRSES (Action No. 318718). Eduardo Ruiz Barlett was funded by Instituto Antártico Argentino. Funding from PICT 2011-1320-ANPCyT to Irene Schloss is acknowledged.

References

1. Turner J, Lu H, White I, King JC, Phillips T, Hosking JS, et al. Absence of 21st century warming on Antarctic Peninsula consistent with natural variability. Nature. 2016 Jul 21;535(7612):411–5.

2. Vaughan DG, Marshall GJ, Connolley WM, Parkinson C, Mulvaney R, Hodgson DA, et al. Recent rapid regional climate warming on the Antarctic Peninsula. Clim Change. 2003;60(3):243–74.

3. Meredith MP, King JC. Rapid climate change in the ocean to the west of the Antarctic Penisula during the second half of the twentieth century. Geophysical Research Letters. 2005;32(L19604):10.1029/2005GL024042.

4. Stammerjohn SE, Martinson DG, Smith RC, Ianuzzi RA. Sea ice in the western Antarctic Peninsula region: spatio-temporal variability from ecological and climate change perspectives. Deep-Sea Research II. 2008;55.

5. Meredith MP, Stefels J, van Leeuwe M. Marine studies at the western Antarctic Peninsula: Priorities, progress and prognosis. Deep Sea Research Part II: Topical Studies in Oceanography. 2017 May;139:1–8.

6. Cook AJ, Fox AJ, Vaughan DG, Ferrigno JG. Retreating Glacier Fronts on the Antarctic Peninsula over the Past Half-Century. Science. 2005;308(5721):541–4.

7. Cook AJ, Holland PR, Meredith MP, Murray T, Luckman A, Vaughan DG. Ocean forcing of glacier retreat in the western Antarctic Peninsula. Science. 2016 Jul 15;353(6296):283–6.

8. Hodson A, Nowak A, Sabacka M, Jungblut A, Navarro F, Pearce D, et al. Climatically sensitive transfer of iron to maritime Antarctic ecosystems by surface runoff. Nature Communications. 2017 Feb 15;8:ncomms14499.

9. Monien D, Monien P, Brünjes R, Widmer T, Kappenberg A, Busso AAS, et al. Meltwater as a source of potentially bioavailable iron to Antarctica waters. Antarctic Science. 2017 Jun;29(3):277–91.

10. Marshall GJ. Trends in the Southern Annular Mode from Observations and Reanalyses. Journal of Climate. 2003;16:4134–43.

11. Rignot E, Casassa G, Gogineni P, Krabill W, Rivera A, Thomas R. Accelerated ice discharge from the Antarctic Peninsula following the collapse of Larsen B ice shelf. Geophys Res Lett. 2004 Sep 1;31(18):L18401.

12. Pritchard HD, Vaughan DG. Widespread acceleration of glaciers on the Antarctic Peninsula. Journal of Geophysical Research. 2007;112(F03S29).

13. Pritchard HD, Ligtenberg SRM, Fricker HA, Vaughan DG, Broeke MR van den, Padman L. Antarctic ice-sheet loss driven by basal melting of ice shelves. Nature. 2012;484:502–5.

14. Osmanoğlu B, Braun M, Hock R, Navarro F. Surface velocity and ice discharge of the ice cap on King George Island, Antarctica. Annals of Glaciology. 2013;54(63):111–9.

15. Falk U, Lopez D, Silva-Busso A. Multi-year analysis of distributed glacier mass balance modelling and equilibrium line altitude on King George Island, Antarctic Peninsula. The Cryosphere. 2017;submitted.

16. Schloss IR, Wasilowska A, Dumont D, Almandoz GO, Hernando MP, Michaud-Tremblay C-A, et al. On the phytoplankton bloom in coastal waters of southern King George Island (Antarctica) in January 2010: An exceptional feature? Limnol Oceanogr. 2014 Jan 1;59(1):195–210.

17. Huss M, Farinotti D. A high-resolution bedrock map for the Antarctic Peninsula. The Cryosphere. 2014;8:1261–73.

18. Hawkings JR, Wadham JL, Tranter M, Raiswell R, Benning LG, Stathan PJ, et al. Ice sheets as a significant source of highly reactive nanoparticulate iron to the oceans. Nature Communications. 2014;5(3929).

19. Klöser H, Ferreyra G, Schloss I, Mercuri G, Laturnus F, Curtosi A. Hydrography of Potter Cove, a Small Fjord-like Inlet on King George Island (South Shetlands). Estuarine, Coastal and Shelf Science. 1994 May 1;38(5):523–37.

20. Schloss IR, Ferreyra GA, Curtosi A, Kloser H, Mercuri G, Pinola E. Factors governing phytoplankton and particulate matter variation in Potter Cove, King George Island Antarctica. In: Battaglia B, Valencia J, Walton DWH, editors. Antarctic Communities. Cambridge, U.K.: Cambridge University Press; 1997. p. 135–41.

21. Falk U, Gieseke H, Kotzur F, Braun M. Monitoring snow and ice surfaces on King George Island, Antarctic Peninsula, with high-resolution TerraSAR-X time series. Antarctic Science. 2016;28:135–49.

22. Poigner H, Monien P, Monien D, Kriews M, Brumsack H-J, Wilhelms-Dick D, et al. Influence of the porewater geochemistry on Fe and Mn assimilation in Laternula elliptica at King George Island (Antarctica). Estuarine, Coastal and Shelf Science. 2013 Dec 20;135:285–95.

23. Monien P, Lettmann KA, Monien D, Asendorf S, Wölfl A-C, Lim CH, et al. Redox conditions and trace metal cycling in coastal sediments from the maritime Antarctic. Geochimica et Cosmochimica Acta. 2014 Sep 15;141:26–44.

24. Ardelan MV, Holm-Hansen O, Hewes CD, Reiss CS, Silva NS, Dulaiova H, et al. Natural iron enrichment around the Antarctic Peninsula in the Southern Ocean. Biogeosciences. 2010 Jan 5;7(1):11–25.

25. Hopkinson BM, Mitchell BG, Reynolds, R.A., Wang, H., Selph KE, Measures CI, et al. Iron limitation across chlorophyll gradients in the southern Drake Passage: Phytoplankton responses to iron addition and photosynthetic indicators of iron stress. Limnology and Oceanography. 52(6):2540–54.

26. Schloss IR, Abele D, Moreau S, Demers S, Bers AV, González O, et al. Response of phytoplankton dynamics to 19-year (1991–2009) climate trends in Potter Cove (Antarctica). Journal of Marine Systems. 2012 Apr 1;92(1):53–66.

27. Deregibus D, Quartino ML, Campana GL, Momo FR, Wiencke C, Zacher K. Photosynthetic light requirements and vertical distribution of macroalgae in newly ice-free areas in Potter Cove, South Shetland Islands, Antarctica. Polar Biol. 2016 Jan 1;39(1):153–66.

28. Abele D, Vazquez S, Buma AGJ, Hernandez E, Quiroga C, Held C, et al. Pelagic and benthic communities of the Antarctic ecosystem of Potter Cove: Genomics and ecological implications. Marine Genomics. 2017 Jun;33:1–11.

29. Mackensen A, Nam S-I. Taxon-specific epibenthic foraminiferal d18O in the Arctic Ocean: Relationship to water masses, deep circulation, and brine release. Micropaleontology. 2014;113:34–43.

30. Meredith MP, Venables HJ, Clarke A, Ducklow H, Erickson M, Leng MJ, et al. The Freshwater System West of the Antarctic Peninsula: Spatial and Temporal Changes. Journal of Climate. 2013;26:1669–84.

31. Khim B-K, Park B-K, Yoon HI. Oxygen isotopic compositions of seawater in the Maxwell Bay of King George Island, West Antarctica. Geoscience Journal. 1997;1(2):115–21.

32. Simoes JC, Ferron FA, Bernardo RT, Aristarain AJ, Stievenard M, Pourchet M, et al. Ice core study from the King George Island, South Shetlands, Antarctica. Pesquisa Antarctica Brasileira. 2004;4:9–23.

33. Ming Y. A preliminary study on oxygen isotope of ice cores of Collins Ice Cap, King George Island, Antarctica. Chinese Journal of Polar Science. 1997;8(1):65–71.

34. Meredith MP, Wallace MI, Stammerjohn SE, Renfrew IA, Clarke A, Venables HJ, et al. Changes in the freshwater composition of the upper ocean west of the Antarctic Peninsula during the first decade of the 21st century. Progress in Oceanography. 2010;87:127–43.

35. Falk U, Sala H. Winter Melt Conditions of the Inland Ice Cap on King George Island, Antarctic Peninsula. Erdkunde. 2015;341–363.

36. Reijmer CH, Hock R. A distributed energy balance model including a multi-layer subsurface snow model. Journal of Glaciology. 2008;54(184):61–72.

37. Brown PJ, Meredith MP, Jullion L, Naveira Garabato A, Torres-Valdés S, Holland P, et al. Freshwater fluxes in the Weddell Gyre: results from δ18O. Philos Trans A Math Phys Eng Sci [Internet]. 2014 Jul 13 [cited 2017 Sep 6];372(2019). Available from: http://www.ncbi.nlm.nih.gov/pmc/articles/PMC4032514/

38. Fuentes V, Alurralde G, Meyer B, Aguirre GE, Canepa A, Wölfl A-C, et al. Glacial melting: an overlooked threat to Antarctic krill. Scientific Reports. 2016 Jun 2;6:srep27234.

39. Sahade R, Lagger C, Torre L, Momo F, Monien P, Schloss I, et al. Climate change and glacier retreat drive shifts in an Antarctic benthic ecosystem. Science Advances. 2015 Nov 1;1(10):e1500050.

40. Ahn I-Y, Moon H-W, Jeon M, Kang S-H. First record of massive blooming of benthic diatoms and their association with megabenthic filter feeders on the shallow seafloor of an Antarctic Fjord: Does glacier melting fuel the bloom? Ocean Sci J. 2016 Jun 1;51(2):273–9.

41. Clem KR, Fogt RL. Varying roles of ENSO and SAM on the Antarctic Peninsula climate in austral spring. Journal of Geophysical Research. 2013;118(20):11481–92.

Figure captions

Figure 1. Maps showing location and bathymetry of Potter Cove, Maxwell Bay and the environs of King George Island at the northern end of the Antarctic Peninsula. Panels focus on progressively smaller scales, clockwise from top left. Arrows indicate Bays and Coves as labelled. Areas marked in brown denotes land not covered by ice; this is not necessarily bedrock but includes surfaces with soil formation, sand and rubble. Blue lines in lower left panel denote the paths of meltwater streams.

Figure 2. Perspective maps of (a) salinity, (b) δ^{18}O, (c) sea ice melt, (d) meteoric water across Maxwell Bay and Potter Cove. Data are from samples collected on February 16th 2013.

Figure 3. Salinity versus δ^{18}O for samples collected across the full period of fieldwork presented here. Note the expanded scale for February 11 (Figure 3b) to incorporate the very fresh, isotopically light waters present then, and for February 16 (Figure 3d) to illustrate the conditions on the Peninsula shelf outside Maxwell Bay, as reflected in the 2010 ANDREX data (red and blue asterisks). In Figure 3c, M denotes sea ice melting, F denotes sea ice freezing, and MW denotes addition of meteoric water.

Figure 4. Salinity in Potter Cove for (a) February 6th 2013, (b) February 11th 2013, (c) February 13th, 2013 and (d) February 16th, 2013. Note in particular the very fresh surface layer present on February 11th.

Figure 5. As per Figure 4, but for δ^{18}O. Note in particular the very isotopically light surface layer present on February 11th.

Figure 6. As per Figure 4, but for meteoric water percentage calculated according to Equation 1. Note in particular the very high levels of meteoric water present on February 11th.

Figure 7. Turbidity (NTU) averaged over the upper 3m of Potter Cove during the sequence of measurements. Note that the spatial extent of elevated turbidity on February 11th (Figure 7b) coincides with the strong prevalence of meteoric water at that time (Figure 6b).

Figure 8. Meteorological and glacial discharge series for the period of January-February 2013. Discharge data are calculated as described in the text. Vertical red bars denote the timing of collection of isotope samples and oceanographic data.

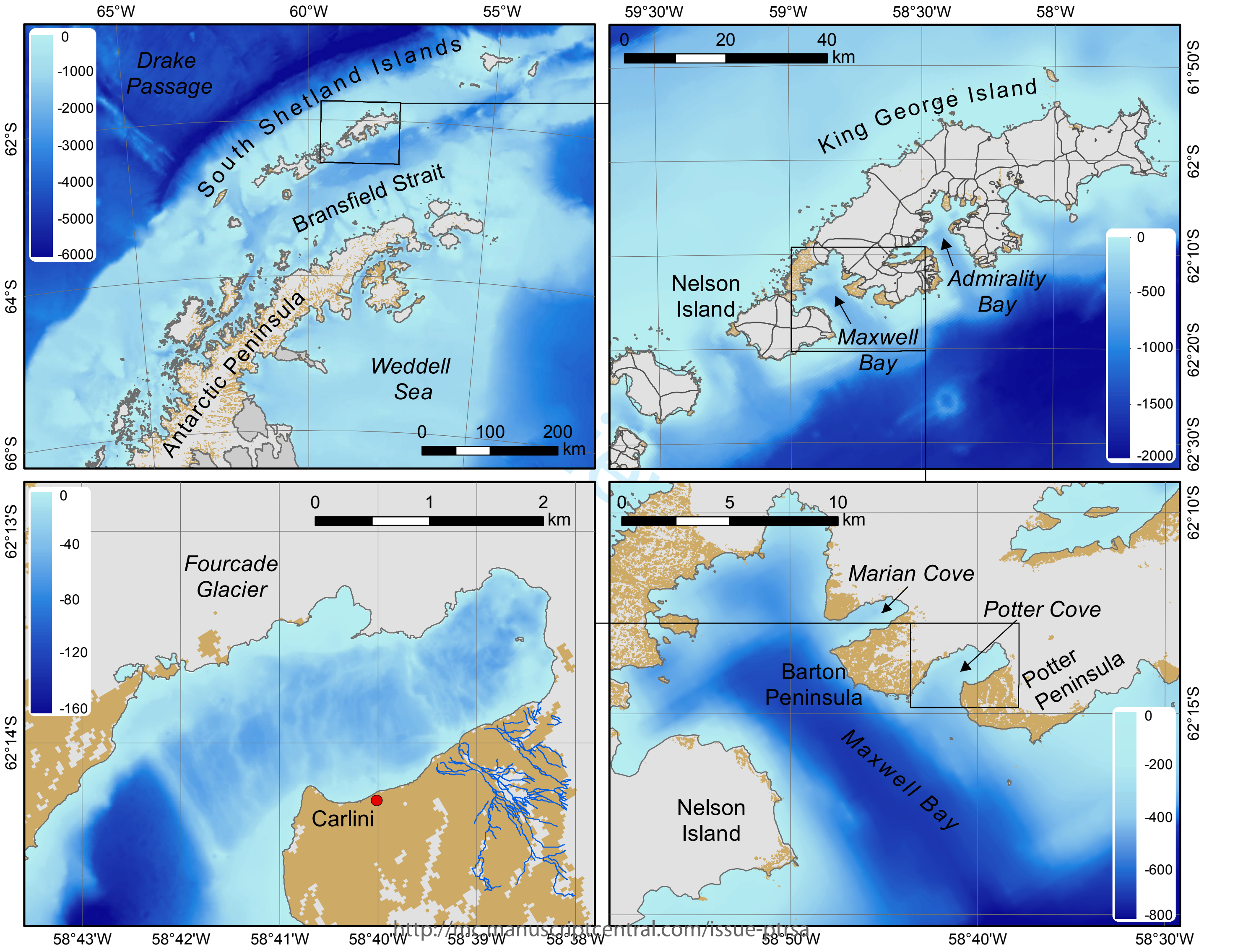
65°W
60°W
55°W
59°30'W
59°W
58°30'W
58°W
Drake Passage
South Shetland Islands
Bransfield Strait
Antarctic Peninsula
Weddell Sea
62°S
64°S
66°S
0
-1000
-2000
-3000
-4000
-5000
-6000
0 100 200 km
King George Island
Nelson Island
Maxwell Bay
Admiralty Bay
0 20 40 km
61°50'S
62°S
62°10'S
62°20'S
62°30'S
0
-500
-1000
-1500
-2000
Fourcade Glacier
Carlini
0 1 2 km
62°13'S
62°14'S
0
-40
-80
-120
-160
58°43'W
58°42'W
58°41'W
58°40'W
58°39'W
58°38'W
Marian Cove
Potter Cove
Barton Peninsula
Potter Peninsula
Maxwell Bay
Nelson Island
0 5 10 km
62°10'S
62°15'S
0
-200
-400
-600
-800
58°50'W
58°40'W
58°30'W

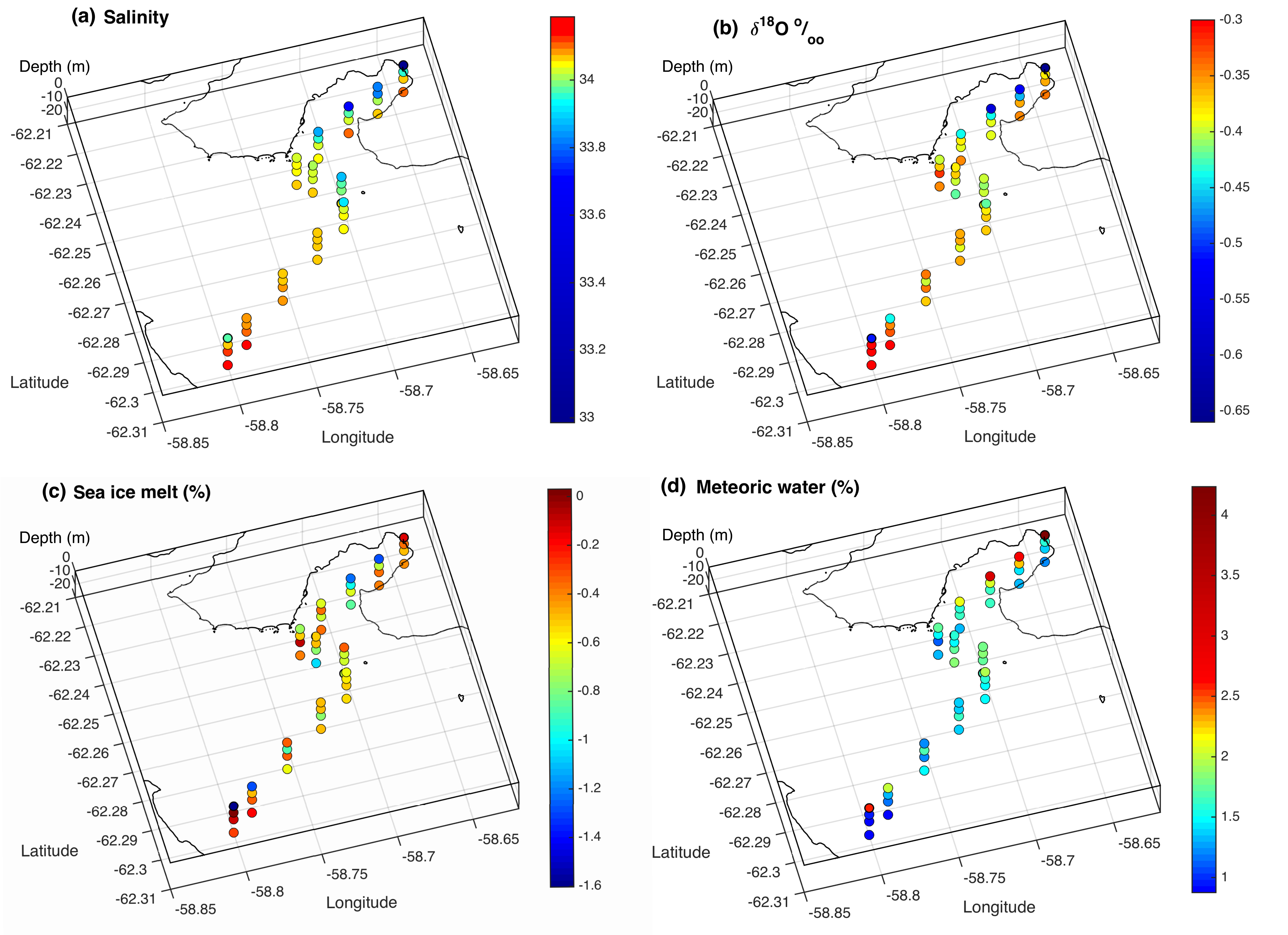
(a) Salinity
Depth (m)
Latitude
Longitude
(b) $\delta^{18}O$ ‰
(c) Sea ice melt (%)
(d) Meteoric water (%)

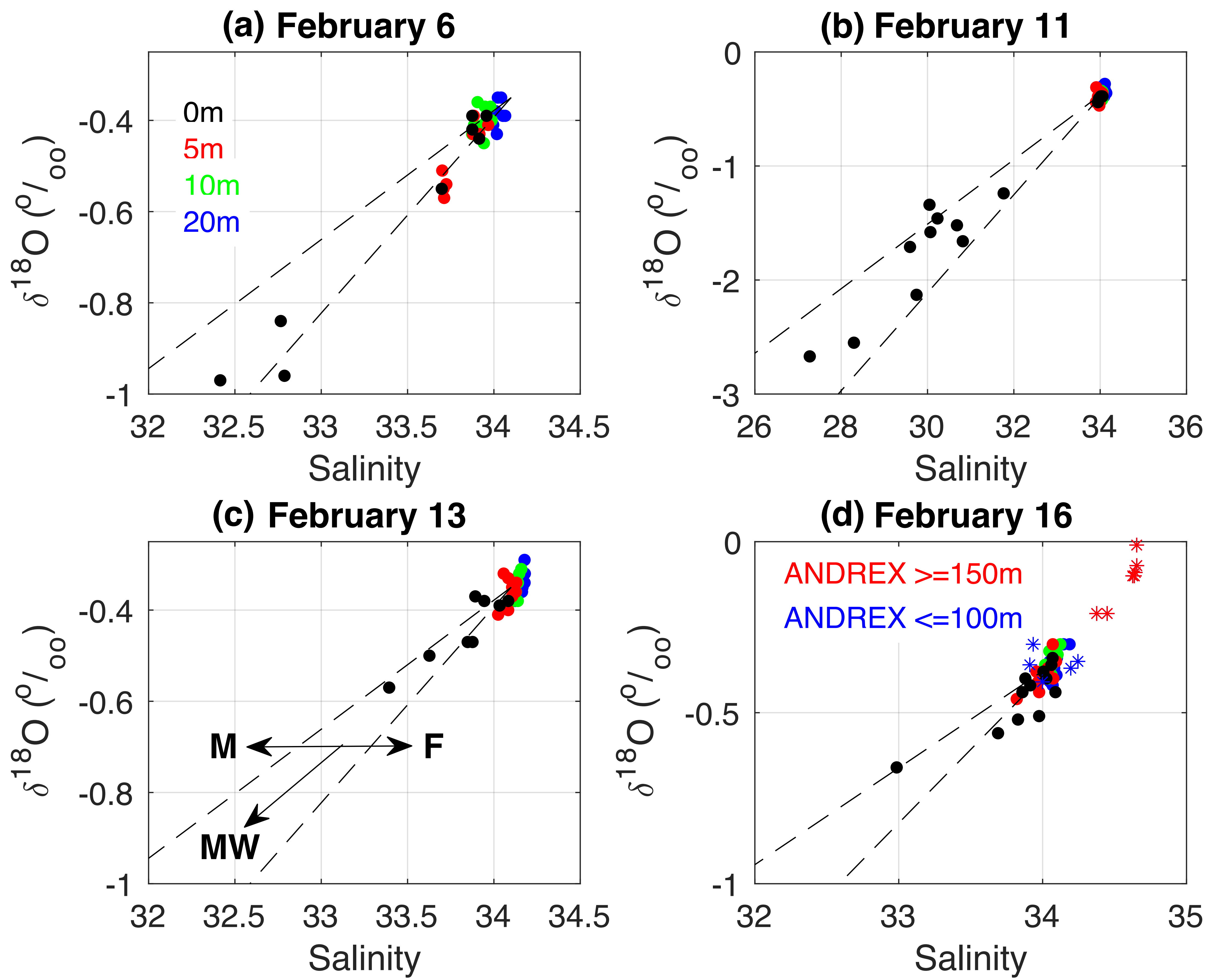
(a) February 6
0m
5m
10m
20m
(b) February 11
(c) February 13
M
F
MW
(d) February 16
ANDREX >=150m
ANDREX <=100m
Salinity
$\delta^{18}O$ ($^o/_{oo}$)
-0.4
-0.6
-0.8
-1
0
-2
-3
-0.5
32
32.5
33
33.5
34
34.5
26
28
30
36
35

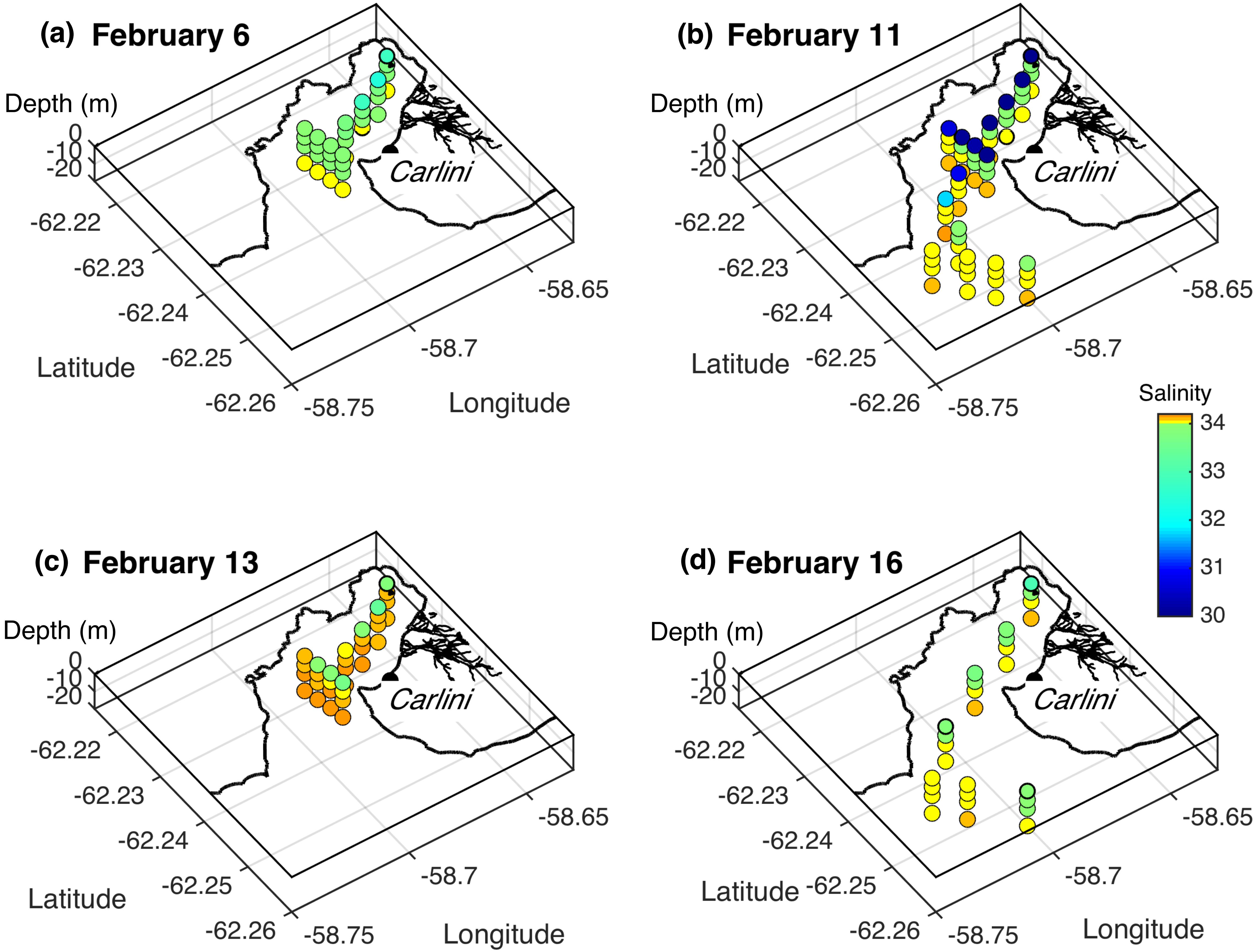
(a) February 6
Depth (m)
0
-10
-20
-62.22
-62.23
-62.24
-62.25
-62.26
Latitude
-58.75
-58.7
-58.65
Longitude
Carlini
(b) February 11
Depth (m)
0
-10
-20
-62.22
-62.23
-62.24
-62.25
-62.26
Latitude
-58.75
-58.7
-58.65
Carlini
Salinity
34
33
32
31
30
(c) February 13
Depth (m)
0
-10
-20
-62.22
-62.23
-62.24
-62.25
-62.26
Latitude
-58.75
-58.7
-58.65
Longitude
Carlini
(d) February 16
Depth (m)
0
-10
-20
-62.22
-62.23
-62.24
-62.25
-62.26
Latitude
-58.75
-58.7
-58.65
Longitude
Carlini

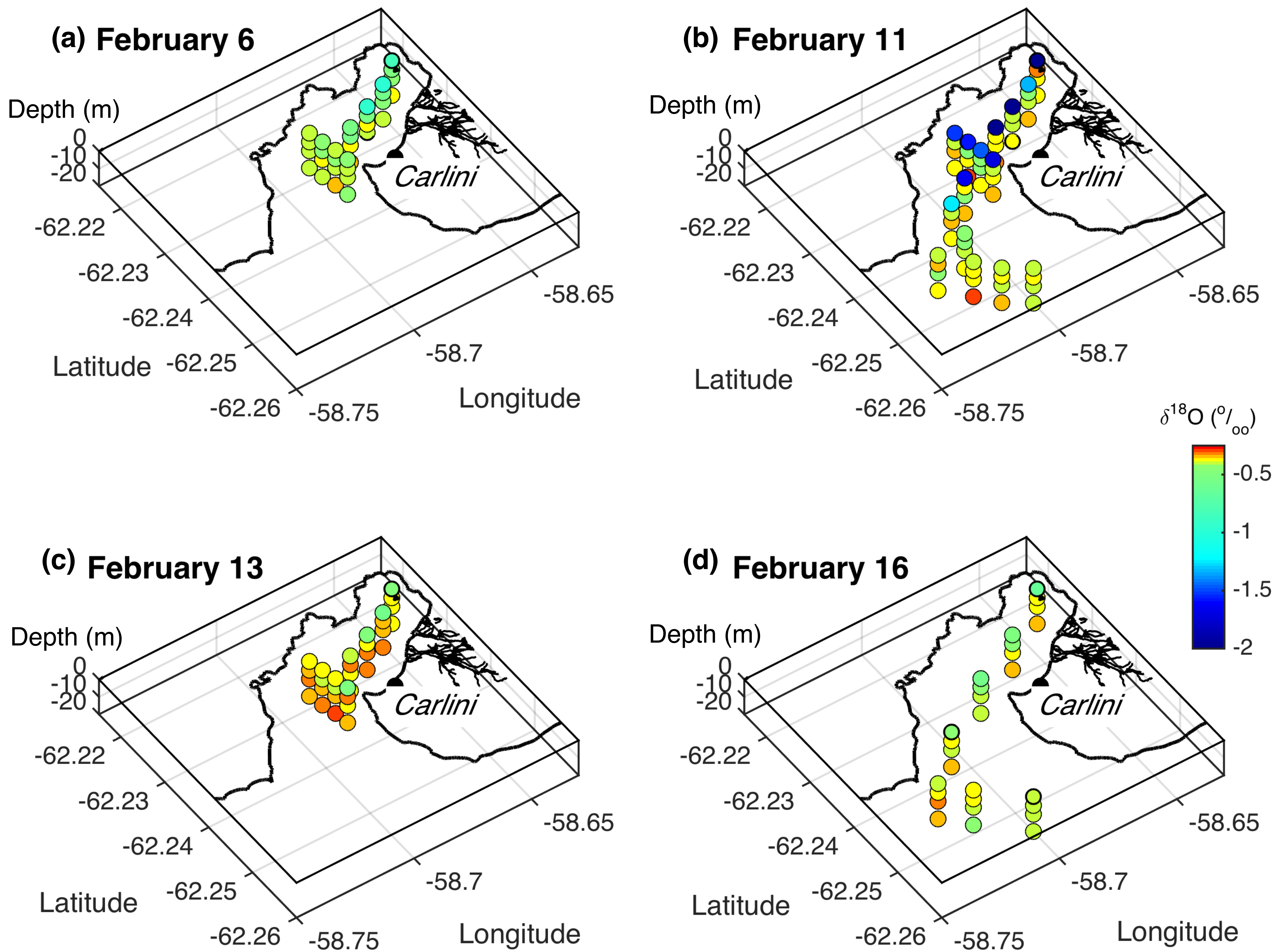
(a) February 6
(b) February 11
(c) February 13
(d) February 16
Depth (m)
0
-10
-20
Carlini
-62.22
-62.23
-62.24
-62.25
-62.26
Latitude
-58.75
-58.7
-58.65
Longitude
$\delta^{18}O$ (°/oo)
-0.5
-1
-1.5
-2

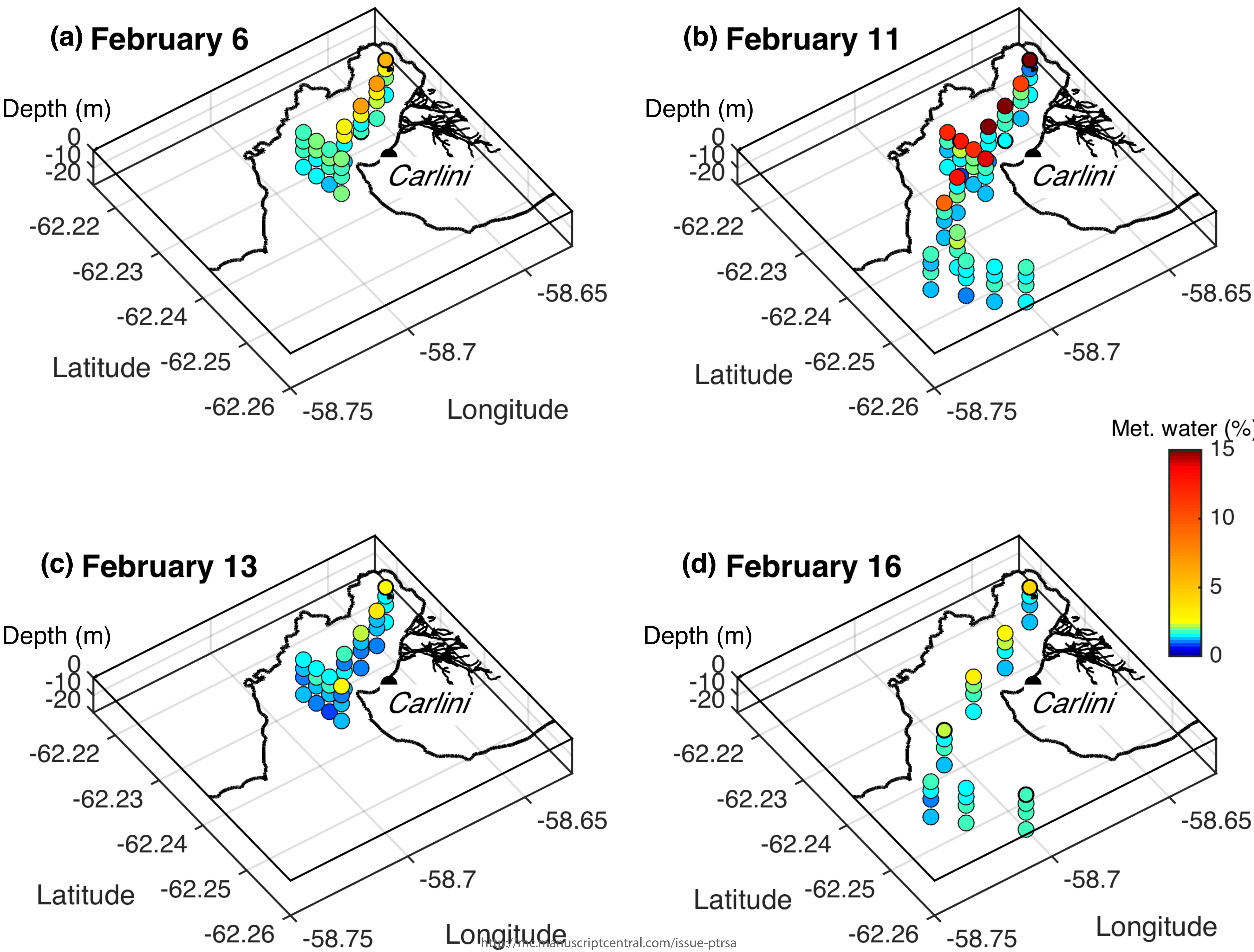
(a) February 6
(b) February 11
(c) February 13
(d) February 16
Depth (m)
0
-10
-20
-62.22
-62.23
-62.24
-62.25
-62.26
Latitude
-58.75
-58.7
-58.65
Longitude
Carlini
Met. water (%)
15
10
5
0

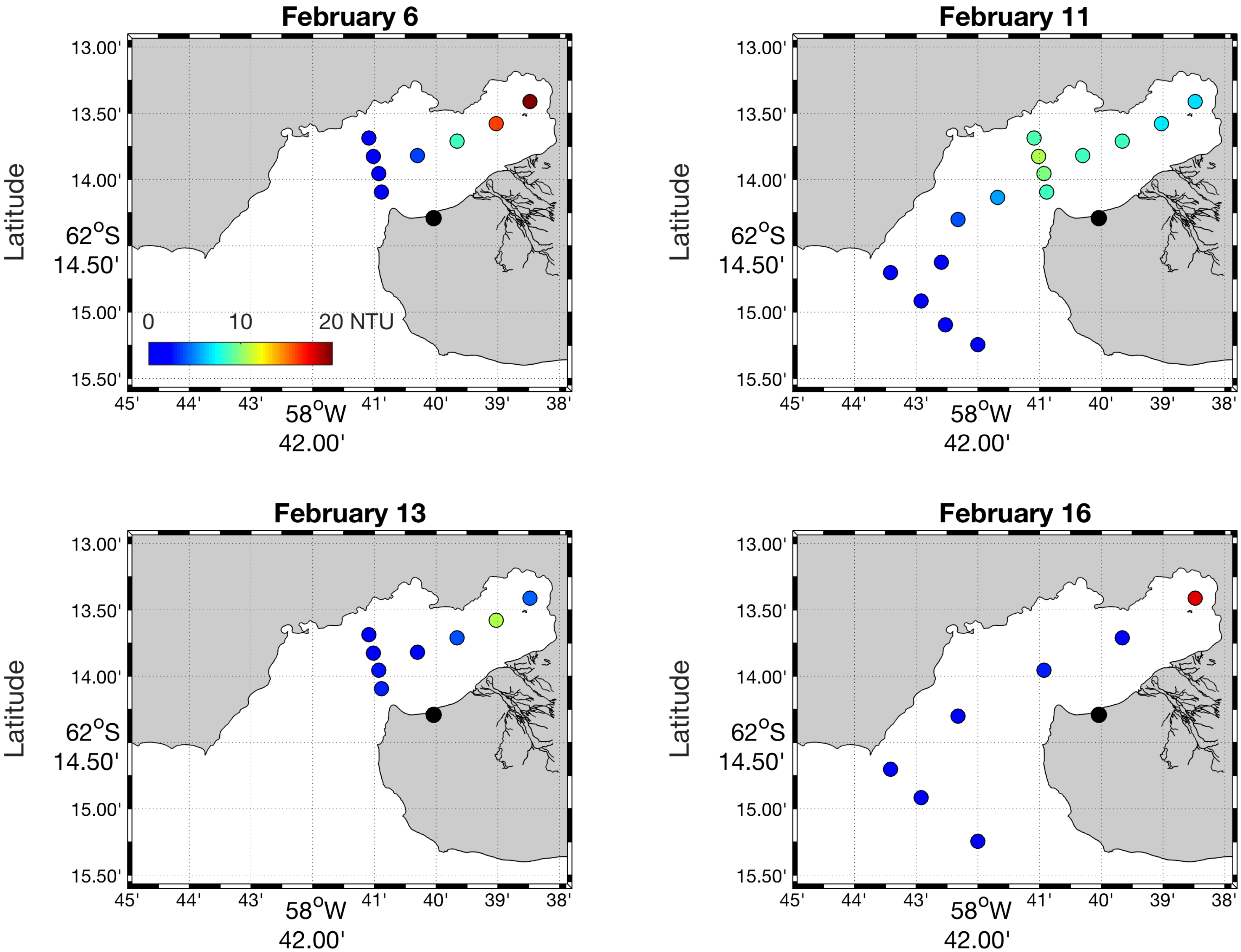
February 6
February 11
February 13
February 16
Latitude
13.00'
13.50'
14.00'
62°S
14.50'
15.00'
15.50'
45'
44'
43'
58°W
42.00'
41'
40'
39'
38'
0
10
20 NTU

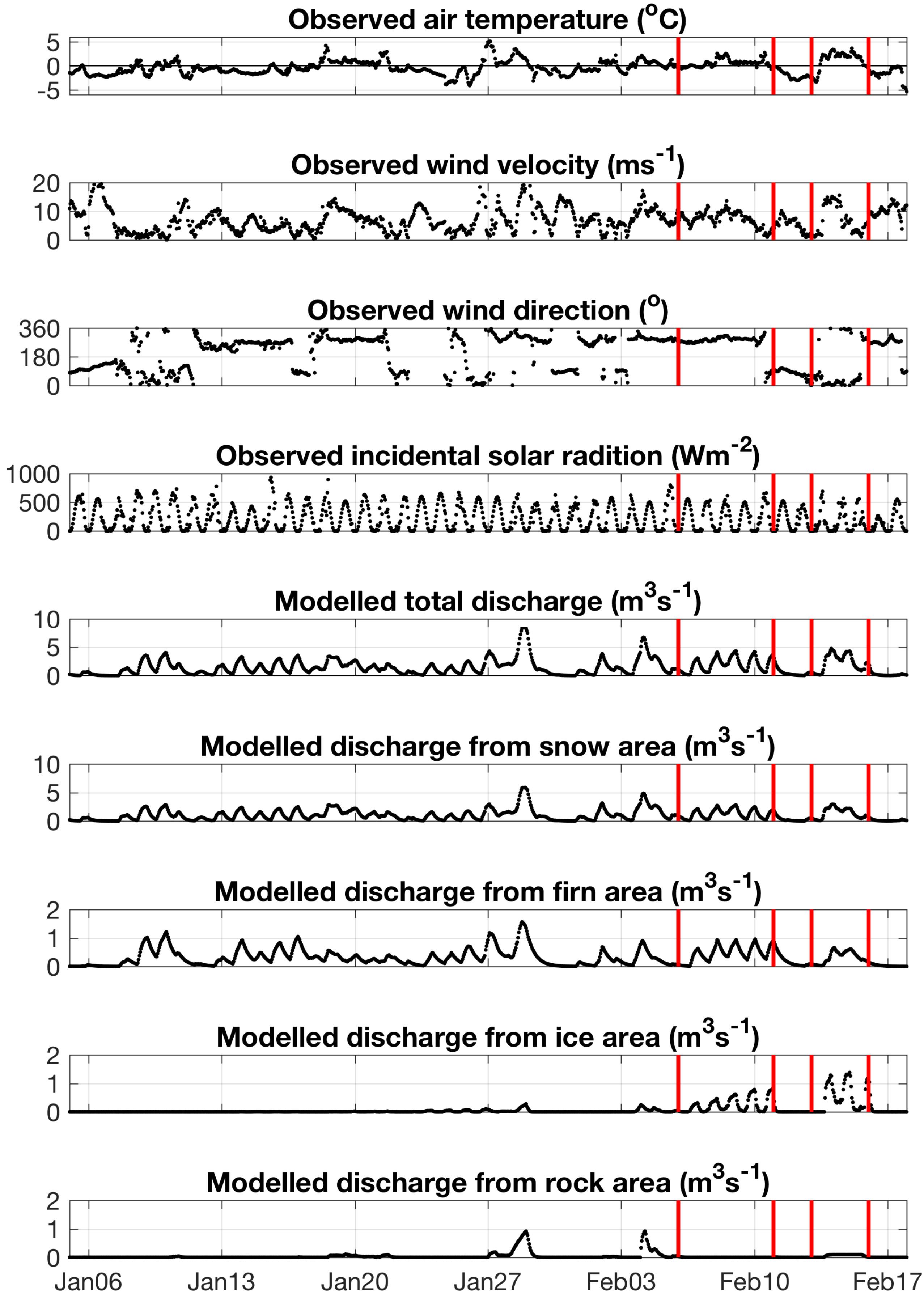
Observed air temperature (°C)
5
0
-5
Observed wind velocity (ms-1)
20
10
0
Observed wind direction (°)
360
180
0
Observed incidental solar radition (Wm-2)
1000
500
0
Modelled total discharge (m3s-1)
10
5
0
Modelled discharge from snow area (m3s-1)
10
5
0
Modelled discharge from firn area (m3s-1)
2
1
0
Modelled discharge from ice area (m3s-1)
2
1
0
Modelled discharge from rock area (m3s-1)
2
1
0
Jan06
Jan13
Jan20
Jan27
Feb03
Feb10
Feb17